Ultra-thin smart electronic skin based on hybrid system-in-foil concept combining three flexible electronics technologies

M. Elsobky✉, Y. Mahsereci, Z. Yu, H. Richter, J. N. Burghartz, J. Keck, H. Klauk and U. Zschieschang

Flexible electronics combined with new materials and fabrication processes offer unique characteristics such as mechanical flexibility, thin-form factor, large area scaling feasibility, and adaptability to irregular surfaces. In this work, a smart electronic skin adopting the hybrid system-in-foil concept is designed to monitor the uniaxial bending of a robotic gripper. The newly designed smart skin contains an array of printed strain gauges, organic thin-film transistor (TFT) addressing circuits and a 20 µm ultra-thin silicon readout chip, all integrated on the same polymeric foil. The silver-ink printed strain gauges achieve a relative resistance sensitivity $\Delta R/R$ of 2% and a gauge factor of 2. In addition, the organic TFT multiplexer containing a three-stage shift register and analogue switches operate at a frequency of 100 Hz and a supply voltage of 3 V. The ultra-thin silicon chip provides the functions of system control, strain gauge readout, analogue-to-digital conversion and serial communication.

Introduction: Recently attention has been directed towards realising sensor systems using the hybrid integration of innovative sensors, organic electronics and silicon chips [1, 2]. This special combination exploits the complementary benefits of the high-performance silicon technology and the large-area printed and organic electronics. However, these sensor systems are still partially rigid, mainly due to the conventional silicon integrated circuit packaging. In this work, a smart electronic skin is designed and fabricated on a flexible substrate to monitor the uniaxial bending of a robotic gripper. The inherently-flexible gripper fingers are able to hold and transport sensitive as well as irregular objects. Integration of an electronic sensing system with the finger flexible structure is desired to extend the robotic functionality and awareness. Figs. 1*a* and 2 show the photo and schematic of the newly designed hybrid system-in-foil (HySiF), which contains an array of printed strain gauges, organic thin-film transistor (TFT) addressing circuits and a 20 µm ultra-thin silicon readout chip. During the uniaxial bending of the finger, its outer surface experiences a non-uniform stress distribution corresponding to the object being held between the gripper fingers. Three gauges are distributed on the upper half of the foil, where the maximum stress is present. The stress-dependent voltage signals from the strain gauges are multiplexed through the low-voltage organic TFT based analogue multiplexer and further processed by the ultra-thin silicon chip.

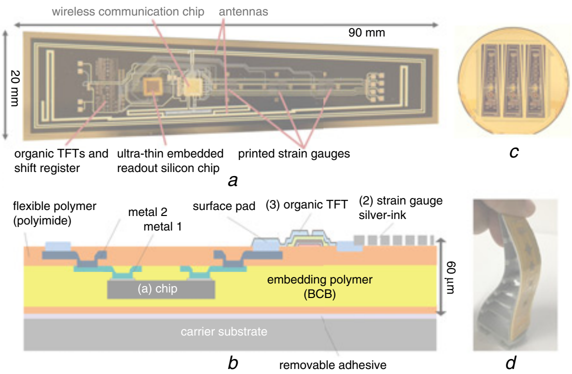

Fig. 1 *The hybrid system-in-foil technology*

a Photo shows HySiF flexible electronic components
b Cross section of HySiF fabrication technology. Fabrication flow has three steps: ultra-thin chip embedding, strain gauge printing, and organic TFT fabrication
c Three HySiF strips were fabricated on 150 mm silicon carrier wafer
d HySiF is released from carrier and mounted on robotic gripper finger using double-sided foam adhesive

Fabrication technology: Fig. 1*b* shows the ultra-thin chip embedding technology (known as ChipFilm Patch (CFP) [3]), which uses a composite substrate of benzocyclobutene (BCB) and polyimide (PI). The BCB is the embedding polymer, which is CMOS-compatible with the capability of fine pitch patterning. The PI provides the necessary mechanical flexibility. The BCB/PI stack is spin-coated on a bow-compensated silicon carrier wafer. The compensation of this stress-induced warpage provides a high degree of surface planarisation which facilitates the embedding of ultra-thin chips and enables better quality for the organic film deposition and silver-ink printing on the substrate surface. A removable adhesive is used to ensure a simple mechanical release of the polymeric foil from the rigid carrier. Two metallisation layers (AlSiCu), in addition to the Au metal pads on the foil surface, are used to connect the embedded silicon chip with the surface components such as the strain gauges and the organic TFT circuit. The strain gauges are fabricated using silver-ink Aerosol Jet® printing at room temperature and multiple overpasses are performed to minimise resistance mismatch. Finally, the inverted-staggered (bottom-gate, top-contact) organic TFTs are manufactured using a near room temperature fabrication process [4]. Only p-channel TFTs are used which are based on the small-molecule organic semiconductor dinaphtho[2,3-b:2′,3′-f]thieno[3,2-b]thiophene. The whole BCB/PI stack is less than 60 µm thick, ensuring good flexibility and ultra-thin form factor.

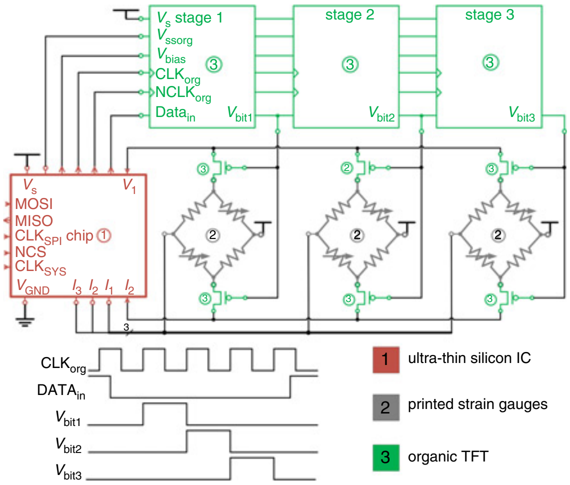

Fig. 2 *Schematic of main HySiF component parts. It includes three printed strain gauges, three-stage organic shift register, three pairs of organic TFT switches and ultra-thin silicon readout chip*

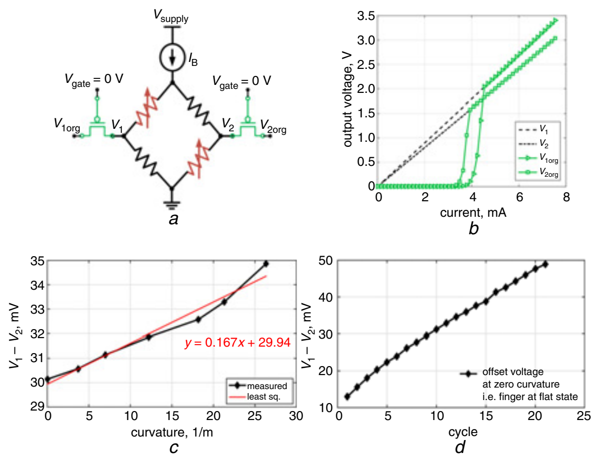

Fig. 3 *Characterization of the printed strain gauge and organic TFT switch*

a Schematic of one strain gauge biased using current source and connected to a pair of organic TFT switches
b Static measurements showing that organic TFT acts as proper switch when $V_{GS} > |V_{th}|$. Gauge resistance here is about 400 Ω
c Measurements show monotonic increase of strain gauge output voltage with increasing bending curvature $(R^2 = 0.97)$
d Offset voltage increases after each bending cycle

Printed sensor: Each strain gauge has an area of $5 \times 5\,mm^2$ with gauge resistance of about 800 Ω and is based on a Wheatstone bridge. Four serpentine-shaped resistors are printed on the BCB/PI substrate, two being strain-sensitive (parallel to the bending direction) and the other two ideally strain-insensitive (perpendicular to the bending direction). For the strain gauge characterisation, a column with a movable rod is used to bend the polymer foil when mounted on the gripper finger. Fig. 3*c* shows the measured strain gauge differential output voltage

($\Delta V = V_1 - V_2$) with the bending curvature. The output voltage is increasing monotonically with increasing the bending curvature (the relationship is ideally linear). The measured ΔV is about 5 mV at a bending radius of 38 mm using 1 mA biasing current. At no bending, a non-zero ΔV is observed (30 mV in this case), which traces back to the resistance mismatch between the four bridge resistors. As shown in Fig. 3*d*, the memory effect in both the gripper finger and glue materials cause the variation of the offset voltage after each bending cycle. Offset compensation is implemented in the embedded ultra-thin silicon chip.

Organic circuit: The static characteristics of the organic TFTs are measured using test devices fabricated on the same BCB/PI substrate, where the extracted threshold voltage (V_{th}) and mobility are −1 V and $1.3\,cm^2/Vs$, respectively. Fig. 3*a* shows a test circuit, in which two organic TFTs are connected to the differential output of a printed strain gauge bridge. Under the proper biasing current, when the strain gauge output voltage exceeds the absolute TFT threshold voltage ($V_{GS} > |V_{th}|$), the organic TFT behaves as an analogue switch (Fig. 3*b*).

Fig. 4 shows the characterisation results of the organic shift register operating at a frequency of 100 Hz. It uses a supply voltage of 3 V and consists of 48 p-channel organic TFTs $(L = 20\,\mu m)$ in an area of $1.4 \times 10.5\,mm^2$. It is designed using a dynamic positive-edge-trigger master-slave flip-flop [5]. In this flip-flop design, the action of a transmission gate switch is performed using two parallel paths. The primary path consists of one p-channel pass transistor, which is used to transfer the high logic level. The secondary path, used for the low logic level, consists of one inverter, one p-channel pass transistor to transfer and another inverter to recover the original logic level. This method introduces additional signal delay; however, it is effective in maintaining the logic voltage levels when using only p-channel organic TFTs. The inverters are based on the biased-load design, which uses a wide driver transistor (channel width $W = 280\,\mu m$) and narrow load transistor $(W = 40\,\mu m)$. The load biasing voltage is generated from the silicon chip (normally at 0 V).

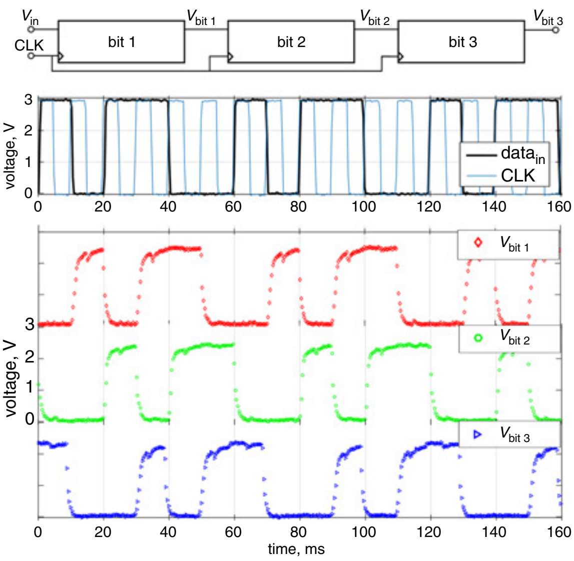

Fig. 4 *Schematic and measurements of three-stage shift register, which is based on dynamic positive-edge-trigger master–slave flip–flop using biased-load inverters*

Sensor readout: The embedded ultra-thin silicon chip is designed in a $0.5\,\mu m$ mixed-signal CMOS technology and is thinned down to $20\,\mu m$ for CFP embedding. It consists of the biasing current generator for the strain gauges, a differential difference amplifier (DDA) for voltage amplification, a 5-bit DAC for offset cancellation and a 10-bit ADC. The closed-loop output voltage of the DDA is given by the following relation:

$$V_{out} = A_c\left(V_1 - V_2 + V_{ref2} - \left(\frac{A_c - 1}{A_c}\right)V_{ref1}\right), \quad (1)$$

where V_1 and V_2 are the strain gauge output voltages, V_{ref1} is a constant reference voltage, V_{ref2} is a variable voltage generated by the DAC. The closed-loop gain A_c is given by $A_c = 1 + R_2/R_1$. Fig. 5 shows the schematic of the sensor readout and its measured 10-bit ADC code versus the input voltage while varying the offset. This proves the effectiveness of the offset cancellation technique.

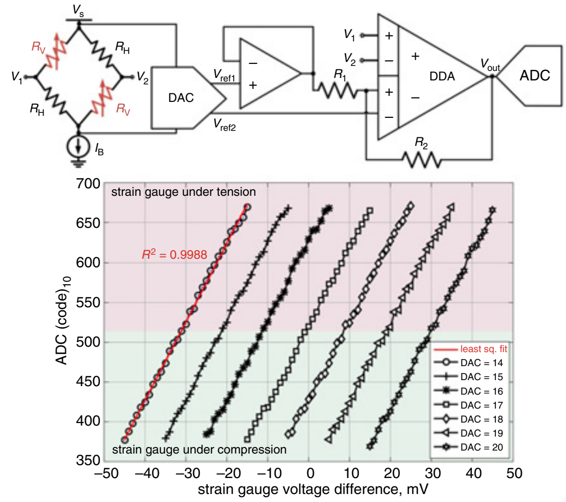

Fig. 5 *Schematic and measurement results of the sensor readout circuit implemented in ultra-thin silicon chip at different offset cancellation voltages*

Conclusion: In this work, we have successfully demonstrated the concept of integrating different flexible electronic components on the same flexible substrate, resulting in a $60\,\mu m$ ultra-thin hybrid foil system. The smart skin for a robotic gripper was chosen as a practical demonstrator. Design and fabrication process flow including all boundary conditions with respect to materials, surface properties, and temperature budget was developed and successfully implemented. In this process flow, all flexible electronic components have been experimentally proved to operate properly using low supply voltage, which is suitable for battery operation. Though there are great challenges in both system design and fabrication techniques, this HySiF opens a brand new aspect for future high-end large area flexible sensor systems.

Acknowledgment: This work was funded by the German Federal Ministry of Education and Research (BMBF) as part of the KoSiF project (#1612000461).

Submitted: *20 December 2017* E-first: *14 February 2018*
doi: 10.1049/el.2017.4682
One or more of the Figures in this Letter are available in colour online.

M. Elsobky, Y. Mahsereci, Z. Yu, H. Richter and J. N. Burghartz (*Institut für Mikroelektronik Stuttgart (IMS CHIPS), Stuttgart, Germany*)

✉ E-mail: elsobky@ims-chips.de

J. Keck (*Hahn-Schickard, Stuttgart, Germany*)

H. Klauk and U. Zschieschang (*Max Planck Institute for Solid State Research, Stuttgart, Germany*)

References

1 Afsar, Y., Moy, T., Brady, N., *et al.*: ‘Large-scale acquisition of large-area sensors using an array of frequency-hopping ZnO thin-film-transistor oscillators’. Int. Solid-State Circuits Conf. – Digest of Technical Papers, 2017, pp. 256–257

2 Moy, T., Huany, L., Rieutort-Louis, W., *et al.*: ‘An EEG acquisition and biomarker-extraction system using low-noise-amplifier and compressive-sensing circuits based on flexible, thin-film electronics’, *J. Solid-State Circuits*, 2017, **52**, pp. 309–321

3 Hassan, M.U., Schomburg, C., Harendt, C., *et al.*: ‘Assembly and embedding of ultra-thin chips in polymers’. Proc. European Microelectronics Packaging Conf., 2013, pp. 1–6

4 Zaki, T., Ante, F., Zschieschang, U., *et al.*: ‘A 3.3 V 6b 100 kS/s current-steering digital-to-analog converter using organic P-type thin-film transistors on glass’, *J. Solid-State Circuits*, 2011, **47**, pp. 292–300

5 Elsobky, M., Elattar, M., Alavi, G., *et al.*: ‘A digital library for a flexible low-voltage organic thin-film transistor technology’, *Org. Electron.*, 2017, **50**, pp. 491–498